This is an *Accepted Manuscript*, which has been through the Royal Society of Chemistry peer review process and has been accepted for publication.

Accepted Manuscripts are published online shortly after acceptance, before technical editing, formatting and proof reading. Using this free service, authors can make their results available to the community, in citable form, before we publish the edited article. This *Accepted Manuscript* will be replaced by the edited, formatted and paginated article as soon as this is available.

You can find more information about *Accepted Manuscripts* in the **Information for Authors**.

An ab initio study of TiS$_3$: a promising electrode material for rechargeable Li and Na ion batteries

Jian Wu,[a] Da Wang,[a] Hao Liu,[b] Woon-ming Lau,[a,b] and Li-Min Liu*[a]

[a]*Beijing Computational Science Research Center, Beijing 100084, China*
[b]*Chengdu Green Energy and Green Manufacturing Technology R&D Center, Chengdu Development Center of Science and Technology of CAEP, Chengdu, Sichuan, 610207, China*

***Corresponding author: *limin.liu@csrc.ac.cn*

Abstract

Titanium trisulfide (TiS$_3$) was recently reported to be highly promising as an electrode material for Li-ion batteries, due to its multielectron processes with high theoretical capacity. However, theoretical work on the performance and mechanism of Li adsorption in bulk and monolayer TiS$_3$ is still lacking. The constraint in the lithium resource also requires replacement by an abundant material such as Na. Using first principles calculations based on density functional theory, the study extensively investigated the electronic structure, adsorption and diffusion properties, capacity and plateaus of Li and Na atoms in bulk and monolayer TiS$_3$. The results reveal that as the thickness in the TiS$_3$ material decreased to a monolayer, a transition from an indirect band gap to a direct band gap was induced. Both the difference charge density and the Bader charge analysis show that a significant charge transfer occurs from Li or Na adatom to its neighboring sulfur atoms. Additionally, in bulk and monolayer TiS$_3$, both Li and Na show two diffusion pathways with a low diffusion barrier, and one pathway can be further enhanced as the TiS$_3$ changes from bulk to monolayer. Moreover, monolayer TiS$_3$ shows a lower energy barrier in Na atom, and also does not cause any problem in the volume expansion in bulk TiS$_3$. In high Li/Na concentration, the Li/Na atom can also diffuse easily, and one diffusion pathway is viable in bulk TiS$_3$, effective for directed diffusion. All these properties are promising for the development of Li and Na batteries based on bulk and monolayer TiS$_3$.

1. Introduction

Developing novel and efficient electrochemical storage devices with high energy densities is vitally important for powering our future society. Among the promising candidates for next-generation high-energy rechargeable batteries, metal sulfides show great potential due to their high electronic conductivity, high theoretical density and low solubility in electrolytes.[1-3] However, over a wide range of materials, there are only a few metal polysulfides that have high sulfur content.

In recent years, titanium polysulfides (TiS_X) have captivated particular attention due to their potential applications as electrode materials, field effect transistors (NR-FET), hydrogen storage devices and in thermoelectric energy conversion.[4-9] Among these polysulfides, crystalline titanium disulfide (TiS_2) with layered structure exhibits excellent cyclability in both electrochemical cells with organic liquid electrolytes and all-solid-state cells with sulfide solid electrolytes.[10-12] Crystalline titanium trisulfide (TiS_3) is another promising candidate because its particles own an even higher theoretical capacity than that of TiS_2 in liquid-type lithium cells. Lindic et al[13] found that the TiS_3 cell exhibited a capacity of 350 mAh g^{-1} for the initial few cycles, and Hayashi et al[14] reported that amorphous TiS_3 particles have a high reversible capacity of 400 mAh g^{-1} in all-solid-state batteries.

On the other hand, the constraint in the lithium resource leads to the requirement to replace lithium with other abundant elements, such as sodium (Na). Various Na based energy storage systems, including Na-ion batteries and Na-ion capacitors, have been widely explored.[15-18] Unfortunately, although a high capacity is generally observed during the first charge in electrochemical reaction of TiS_3 with Na, the capacity cannot be maintained during subsequent cycles owing to the structural decomposition of TiS_3 at high temperature.[19] Therefore, to utilize Na batteries in bulk TiS_3 systems, the study seeks to understand the insertion, diffusion and volume expansion after Na absorbed in bulk TiS_3.

It has been well known that as their thickness decrease to a few layers or even to a monolayer, the structure and electronic properties of certain layered materials change remarkably leading to new and unexpected properties and hence bringing in many important applications.[20] More importantly, few-layer TiS_3 nanoribbons made from exfoliation present remarkable field effect transistors (FET) characteristics, high photoresponse and fast switching rates.[21, 22] However, no experimental and theoretical study has been focused on the mechanism of Li/Na adsorption on monolayer TiS_3. From the theoretical point of view, first-principles computational methods are playing an important role in understanding the electronic structure and the performances of electrode materials.[23-28] This study intends to fill the gap.

In this work, for the first time first principles calculations were used to comparatively examine the Li/Na adsorption and diffusion in bulk and monolayer TiS_3. The phase stability, electronic properties, capacity and plateaus of both bulk and monolayer TiS_3 were carefully investigated. Meanwhile, the difference charge density and the Bader charge analysis were used to study the interaction between Li/Na adatom and its surrounding atoms. The energy barriers for Li and Na migration in bulk and monolayer TiS_3 were also evaluated. These analyses would give us a solid

foundation to better harness TiS_3 as electrode materials for rechargeable Li and Na ion batteries.

2. Methods

The first-principles calculations were performed using DFT calculations as implemented in the Vienna ab initio simulation package (VASP).[29, 30] The exchange-correlation term has been described within the generalized gradient approximation (GGA) parameterized by Perdew-Burke-Ernzerhof (PBE) functional.[31] A kinetic-energy cutoff for plane-wave expansion was set to 360 eV. A 2a ×3b ×1c supercell (where a, b and c are the lattice constants of bulk TiS_3) with a three dimension period boundary condition for bulk, and a 2a × 3b slab with about 15 Å vacuum along the c direction for monolayer TiS_3 were used to simulate the Li and Na adsorption and diffusion y. All the atoms in the unit cell were fully relaxed until the force on each atom was less than 0.01 eV/Å. Electronic minimization was performed with a tolerance of 10^{-6} eV. The Brillouin-zone (BZ)[32] sampling was carried out with a 6×8×1 Monkhorst-Pack grid for 2D sheets and a 6×8×3 Monkhorst-Pack grid for bulk. In order to avoid the disadvantages of severely underestimating band gaps by using the DFT-PBE calculation , the hybrid functional calculations with HSE06[33] were used, which is a better test to give relatively accurate band gaps for a wide range of materials. The van der Waals (vdW) interaction of bulk TiS_3 is corrected by using the DFT-D2 approach.[34] The stability of monolayer TiS_3 is studied by calculating its phonon spectra based on the force constant approach[35] with the package of Phonopy.

To investigate the Li and Na diffusion kinetics, the study used the climbing image nudged elastic band (CI-NEB) method to seek saddle points and minimum energy pathway between the given initial and final positions. Hence, the energy barriers can be calculated. For the analyses, several images were employed between the fixed initial and final configurations. Each image was relaxed until the forces on atom were < 0.01 eV/Å.

3. Results and Discussion
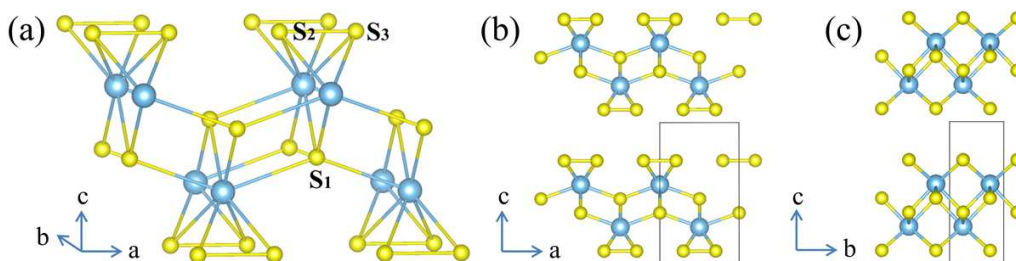
3.1 The structure and stability of TiS_3

Fig. 1 (a) Structure of TiS_3 (formula: $Ti^{4+}[S_2^{2-}]S^{2-}$) extending over about eight unit cells: the blue and yellow balls represent the Ti and S atoms, respectively. S_1 is sulfide (S^{2-}), and S_2 and S_3 are disulfide (S_2^{2-}). (b) and (c) are side views of bulk TiS_3.

A full geometry optimization of both atomic coordinates and lattice parameters for both bulk and monolayer TiS_3 were firstly performed. The optimized values are given in Table 1 together with experimental data. **Fig. 1** shows that two of the three sulfur atoms in one formula unit are present as a single-bonded disulfide ion (S_2^{2-}), and the third sulfur atom is formally sulfide (S^{2-}). Bulk TiS_3 consists of TiS_3 layers attracted by a weak van der Waals interaction with a interlayer spacing of ~3.2 Å. The calculated cell parameters and the interatomic Ti-S and disulfide (S_2^{2-}) distances of bulk TiS_3 agree well with experimental results.[36] (**Table 1**) The atomic positions and cell parameters of monolayer TiS_3 are almost the same as those in the bulk phase.

Table 1 Optimized and experimental lattice parameters, bond length (Å) and band gap (HSE06).

	Bulk	Monolayer	Experiment[36, 37]
a	4.981	4.995	4.958
b	3.391	3.392	3.4006
c	8.910		8.778
$Ti-S_1$	2.64	2.65	2.64
$Ti-S_2$	2.49	2.47	2.49
$Ti-S_4$	2.46	2.44	2.45
$S_2 - S_3$	2.04	2.01	2.04
band gap	0.94	1.02	0.90

For confirmation of the structure stability of monolayer TiS_3, the full phonon dispersion spectrums of the structure along the high-symmetry directions in Brillouin zone were calculated. When a structure is thermodynamically stable, all its phonon frequencies on the k-points in the Brillouin zone should be positive.[38-40] As shown in **Fig. 2**, almost no imaginary vibration frequency appears for the monolayer TiS_3, implying that the monolayer TiS_3 has high phonon stability. Thus, the monolayer TiS_3 should be thermodynamically stable.
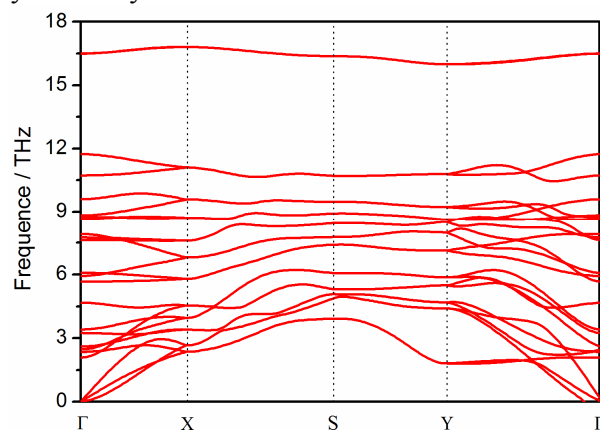

Fig. 2. Calculated phonon branches of monolayer TiS_3 along high-symmetry directions in the Brillouin zone.

3.2 The electronic structure of TiS$_3$

As it is known, the electronic conductivity of a material is extremely correlated with its electronic structures, especially for the ones whose energy band gap is around Fermi level. For comparison, the band structures and total density of states (DOS) of bulk and monolayer TiS$_3$ are shown in **Fig. 3 (a)** and **(b)**, respectively. Based on the calculation with PBE, the bulk TiS$_3$ is an indirect semiconductor with a band gap of 0.14 eV, which is about 0.76 eV smaller than the experimental value of E$_g$ = 0.90 eV. [37] It is well known that pure DFT usually underestimates the band gap of a semiconductor because of the self-interaction error. Therefore the hybrid functional HSE06 was used to examine the band gaps for both bulk and monolayer TiS$_3$ as the hybrid functional can give more accurate band gap readings because of the introduction of the exact change. The calculated band gap of bulk TiS$_3$ with HSE06 is 0.94 eV, which is in good agreement with the reported value above.
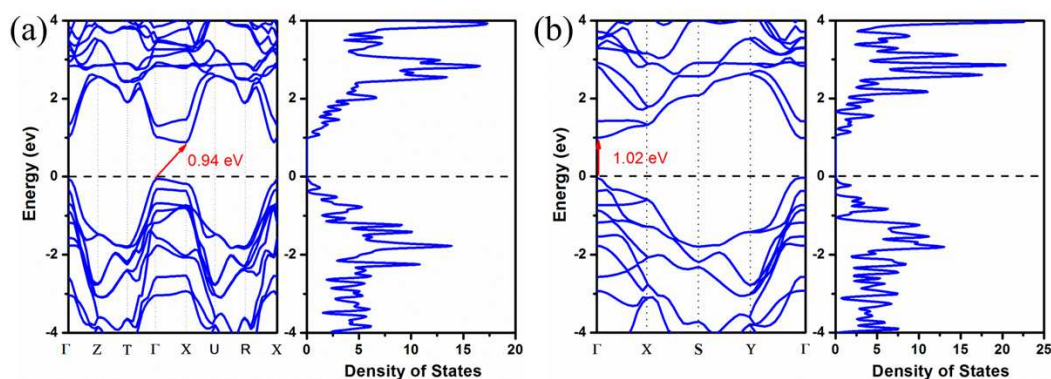

Fig. 3 Band structure and corresponding total density of states (DOS), E$_f$, shown by black dashed lines and dots, for (a) bulk and (b) monolayer TiS$_3$, respectively. The Fermi energy is set to zero. (By HSE06 calculations)

Although the bulk TiS$_3$ is an indirect semiconductor, interestingly, monolayer TiS$_3$ becomes a direct one (see **Fig. 3**). The calculated band gap of monolayer TiS$_3$ is 0.23 eV with PBE, while HSE06 gives a band gap of 1.02 eV, which is about 0.80 eV larger than that of bulk one. Such transition of band structure from indirect to direct has also been observed in other systems, such as MoS$_2$, WS$_2$, and MoSe$_2$, during the exfoliation of the monolayer from the bulk materials.[20, 41] Besides larger surface area, monolayer TiS$_3$ also processes special electronic properties, which may have important applications in battery and other fields.

3.3 TiS$_3$ as Li/Na ion batteries anode

As discussed above, the calculated electronic structure of TiS$_3$ shows that both bulk and monolayer TiS$_3$ are semiconductors with a band gap of about 1 eV, which has potential applications in field effect transistors and optoelectronic switch. To put TiS$_3$ into application as Li/Na ion batteries, we calculated the properties of Li/Na

adsorption and diffusion in bulk and monolayer TiS_3 as follows:

Firstly, the Li/Na binding energy, $E_b(Li/Na)$, between the Li/Na atom and the bulk and monolayer TiS_3 are calculated by the following definition:

$E_b(Li/Na)=E_{tot}(TiS_3)+ E_{tot}(Li/Na)- E_{tot}(TiS_3\text{-}Li/Na)$,

where $E_{tot}(TiS_3\text{-}Li/Na)$ and $E_{tot}(TiS_3)$ are the total energies of Li/Na-adsorbed TiS_3 (bulk or monolayer) and pure TiS_3, respectively. $E_{tot}(Li/Na)$ are the total energies of bulk bcc Li/Na, respectively. If E_b is positive, the lithiation reaction is exothermic (favorable), which indicates the Li/Na atoms tend to bind to the TiS_3. According to this definition, a more positive E_b indicates a more favorable exothermic Li/Na insertion reaction between Li/Na atoms and TiS_3.

A schematic presentation of the atomic configuration of Li/Na adsorbed on monolayer TiS_3 at H, T_1 and T_2 sites, respectively is shown in **Fig 4**. As can be seen in **Fig 4**, there are three different high symmetry sites for both bulk and monolayer TiS_3 i.e. H, T_1 and T_2 sites. The $E_b(Li/Na)$ of these three sites are hence presented in **Table 2**. Meanwhile, the equilibrium bond length between Li/Na and nearest neighbor S atoms for both bulk and monolayer TiS_3, as well as the expansion of lattice parameters c after Li/Na absorbed in bulk TiS_3 were also calculated.
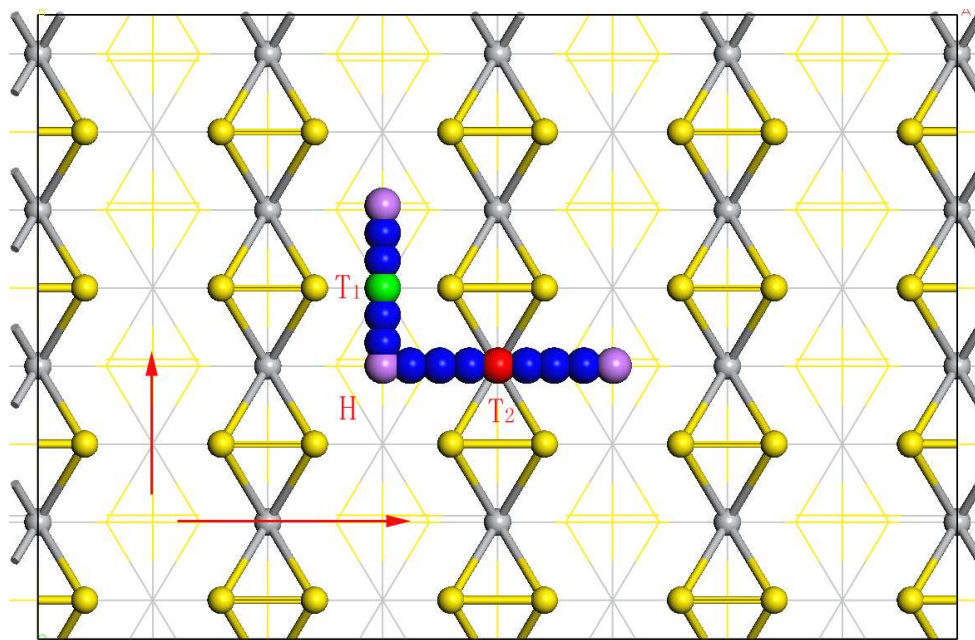

Fig. 4 Top view of the atomic configuration of Li/Na adsorbed on monolayer TiS_3 at H, T_1 and T_2 sites, respectively. The arrows show the diffusion pathway of Li/Na atoms between two neighboring H sites by passing through the T_1 and T_2 sites.

For bulk TiS_3, the six adjacent sulfur atoms form six coordination bonds with Li/Na atom in all three sites. The adatom on site H and T_2 connect to the up layer with two bonds and the lower layer with the other four bonds, while the adatom on T_1 site is in reverse to that on H and T_2 site. The most stable site of adsorbed Li/Na atoms in bulk TiS_3 is the H site, where the Li and Na binding energies are 1.82 and 1.35 eV,

respectively. It should be noted that the Li/Na binding energies and the lattice expansion in c are the same in the T_1 and T_2 sites, because of the equivalent coordination bonds in the bulk. Compared with Li adsorption in bulk TiS_3, the expansion of lattice parameters for Na adsorption is much higher, which will result in the structure deformation of TiS_3 and then the capacitance fading. This is consistent with experimental result that bulk TiS_3 is not suitable as electrodes for Na ion batteries.[19]

Table 2 Binding energies (E_b) of Li/Na absorbed in bulk and monolayer TiS_3 (eV) and the Li/Na-S equilibrium bond length ($d_{Li/Na-S}$) with the nearest neighbor S atoms (Å) at the H, T_1 and T_2 sites, respectively. The subscripts "u" and "d" in the bottom right corner indicate the $d_{Li/Na-S}$ bonding with up and down TiS_3 layer when Li/Na embedded in bulk TiS_3, respectively. Δc means the expansion of lattice parameters c after Li/Na absorbed in bulk TiS_3.

	Monolayer		Bulk	
	Li	Na	Li	Na
(H) E	1.15	1.12	1.82	1.35
Δc			1.04 %	4.17 %
$d_{Li/Na-S}$	2.44	2.81	2.52_d, 2.53_u	2.68_d, 2.67_u
(T$_1$) E	0.69	0.78	1.71	1.18
Δc			1.77 %	6.56 %
$d_{Li/Na-S}$	2.34	2.70	2.44_d, 2.52_u	2.62_d, 2.75_u
(T$_2$) E	0.89	0.9	1.71	1.18
Δc			1.76 %	6.54 %
$d_{Li/Na-S}$	2.46	2.81	2.52_d, 2.44_u	2.75_d, 2.62_u

In the case of monolayer TiS_3, the E_b(Li) for a Li adatom adsorbed on the H, T_1 and T_2 sites are 1.15, 0.69 and 0.89 eV, respectively (see Table 2). The most stable site of Li/Na adatom is the center of the four neighbor S atoms forming four coordination bonds in the same plane (H site). The equilibrium bond length of Li-S (d_{Li-S}) is 2.44 Å, and the adsorbed Li atom is about 0.68 Å above the TiS_3 layer. On the T_2 site, Li is adsorbed on one Ti atom with a distance of 3.01 Å, forming four coordination bonds with slightly stretched d_{Li-S} of 2.46 Å and greatly enlarged h of 1.33 Å. In the case of T_1 site, Li is also adsorbed on one Ti atom with a distance of 5.96 Å but bonded with only two nearest neighbor S atoms with d_{Li-S} of 2.34 Å, and the h is further enlarged (1.61 Å) compared with Li adatom on T_2 site.

As with the Li adatom, study on Na adatom on the monolayer TiS_3 surface at H, T_1 and T_2 sites was also carried out and the results are presented in table 2. In general, the Na-S equilibrium bond lengths (d_{Na-S}) for different position are elongated on average by 0.36 Å compared with d_{Li-S} due to the larger atomic radius of Na.

To understand the bonding nature of Li/Na adsorbed in the bulk and monolayer

TiS$_3$, the study calculated the charge density difference, $\Delta\rho(r)$, as expressed in the following formula,

$$\Delta\rho(r) = \rho_{Li/Na-TiS_3}(r) - \rho_{Li/Na}(r) - \rho_{TiS_3}(r),$$

where $\rho_{Li/Na-TiS_3}(r)$ represents the charge density of the Li/Na adsorbed TiS$_3$ system, $\rho_{TiS_3}(r)$ is the charge density of the TiS$_3$ (without Li/Na), and $\rho_{Li/Na}(r)$ is the charge density of isolated Li/Na atoms located at the same position as in the total system.
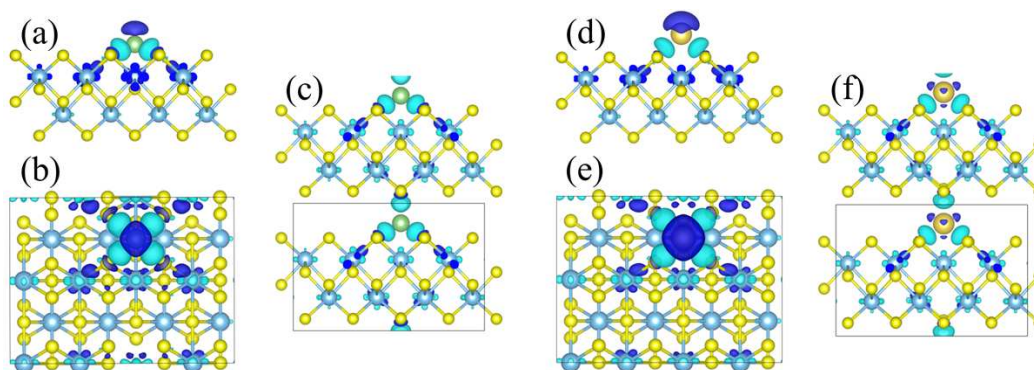

Fig. 5 Isosurface (0.002 e Å), wathet blue for $\Delta\rho > 0$ and dark blue for $\Delta\rho < 0$ of the difference charge density $\Delta\rho$ for the most stable configuration of Li adsorbed at the H site in the (a),(b) monolayer and (c) bulk TiS$_3$; and Na located at the H site in the (d), (e) monolayer and (f) bulk TiS$_3$.

Fig. 5 shows the charge density difference of Li/Na atoms located at the H site in bulk and monolayer TiS$_3$. For the Li adsorbed at the H site on the monolayer TiS$_3$, there is a net loss of electronic charge right above the Li, whereas there is a net gain of electronic charge in the intermediate region between Li and four adjacent sulfur atoms, indicating a significant charge transfer from the adsorbed Li to its nearest neighbor S atoms. The Bader charge analysis[42, 43] was performed to quantitatively estimate the amount of charge transfer between the adsorbed Li and the TiS$_3$. The Bader charger state of a Li atom adsorbed at the H site on the monolayer TiS$_3$ is $+0.8678 |e|$, and the averaged Bader charge state of the four sulfur atoms next to the Li is $-0.1488 |e|$. In the case of the Li located at the H site in the bulk TiS$_3$, the Bader charge state of Li atom is $+0.8602 |e|$, and the net gain of electronic charge for each adjacent sulfur atoms is $-0.1298 |e|$. The total electronic transfer from Li and its

nearest sulfur atoms in bulk TiS_3 is $-0.1836|e|$ higher than that in monolayer TiS_3, leading to a higher binding energy between Li and S in bulk TiS_3. Similar results can be found in Na adatom case. These results suggest that the interaction between the adsorbed Li/Na atom and its nearest neighbor sulfur atoms is predominantly ionic, and the valence electrons of the adsorbed Li/Na atoms are mainly transferred to the neighbor sulfur atoms.
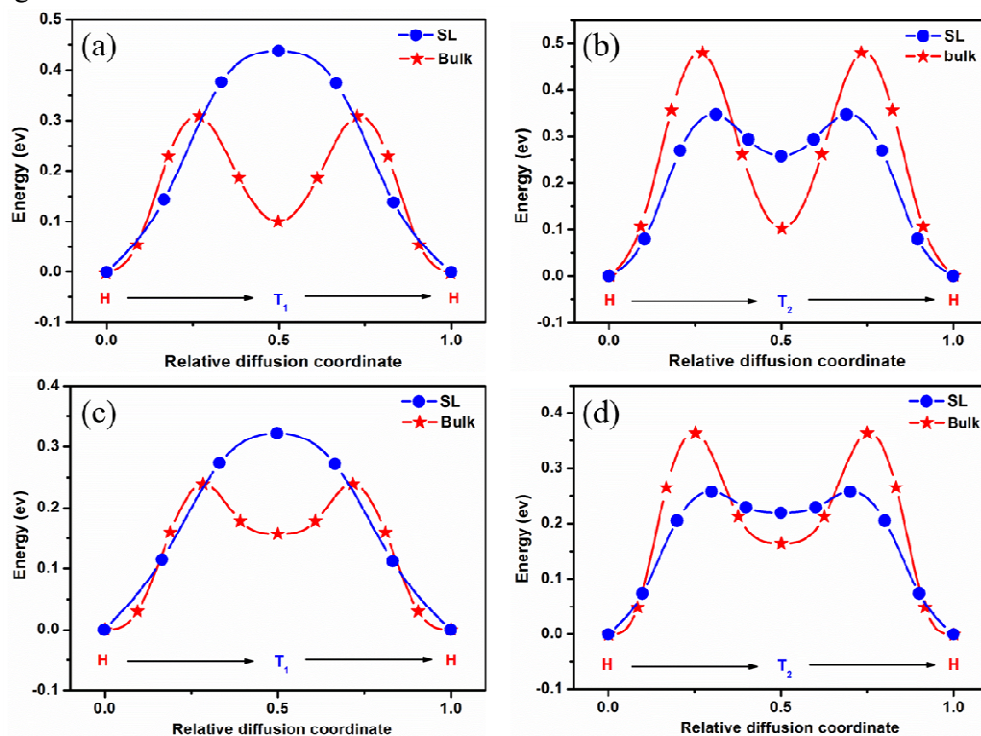

Fig. 6 Energy barrier (∇E) for Li ((a) and (b)) and Na ((c) and (d)) atoms diffuse along H-T_1-H and H-T_2-H pathways in bulk and monolayer TiS_3, respectively.

As previously confirmed, Li and Na atoms tend to be adsorbed at the H site in both bulk and monolayer. Hence, Li/Na atoms could diffuse from an H site to a neighboring H site by passing through T_1 or T_2 site (see **Fig. 4**). Results of the investigation of diffusing barriers of Li/Na atoms through either site in both bulk and monolayer TiS_3 are shown in **Fig. 6** and **Table 3**.

Table 3 Energy barriers (∇E) for Li and Na diffusion in bulk and monolayer TiS_3 (eV).

∇E	Monolayer		Bulk	
	Li	Na	Li	Na
H-T_1-H	0.44	0.32	0.31	0.24
H-T_2-H	0.35	0.26	0.48	0.36

The diffusion barrier of Li/Na along the H-T_2-H diffusion pathway decreases

from 0.48/0.36 to 0.35/0.26 eV as the thickness decreased to a monolayer, respectively, which reveals that Li/Na can diffuse faster on monolayer TiS_3 than in bulk TiS_3. However, on monolayer TiS_3, the calculated energy barriers (∇E) of Li/Na along the H-T_1-H diffusion pathway are slightly higher compared with that in bulk TiS_3. This can be attributed to the fact that the coordination bonds in monolayer TiS_3 changes from four coordination bonds (H site) to two coordination bonds (T_1 site) and then back to four coordination bonds (H site) during the Li/Na diffusion process. The changes of coordination bonds result in a larger energy barriers. On the other hand, no coordination bonds change in the case of bulk TiS_3. These results indicate that the Li/Na mobility can be further enhanced along the H-T_2-H pathway by decreasing the thickness of TiS_3 to a monolayer. In addition, the energy barrier of Na is smaller than that of Li regardless of the thickness and the pathways, which can be attributed to the larger Na-S chemical bonds than Li-S and thus less constraint.
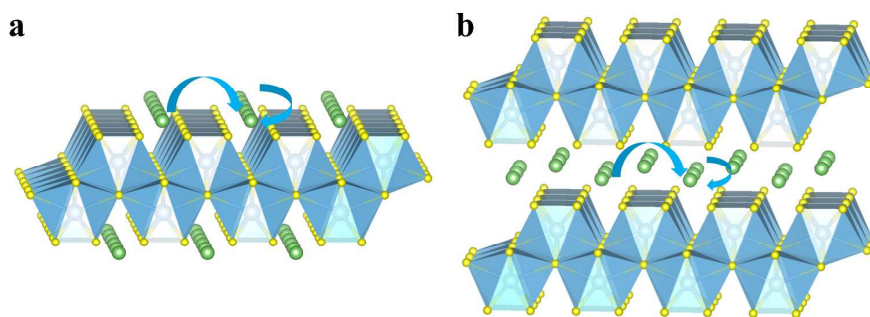

Fig. 7 Schematic of the diffusion pathway of Li/Na atoms between two neighboring H sites by passing through the T_1 and T_2 sites in bulk and monolayer TiS_3 with Li/Na atoms absorbed the whole H sites except an unoccupied H site, respectively.

To further understand the Li/Na diffusion in the case of high Li/Na concentrations, we have investigated the energy barriers for Li/Na atoms diffusion along H-T_1-H and H-T_2-H pathways in bulk and monolayer $Li/NaTiS_3$ systems, respectively. A schematic of the diffusion pathways are shown in **Fig. 7** and the calculated diffusing barriers are summarized in **Fig. 8** and **Table. S1**. It is shown that in high Li/Na concentration, energy barriers for Li/Na atoms diffuse along H-T_1-H and H-T_2-H pathways in bulk and monolayer TiS_3 are about 0.2 eV higher than that in low concentration cases. Moreover, it is interesting to find that the diffusion barrier of Na along the H-T_2-H diffusion pathway in bulk TiS_3 is closed due to the very high diffusion barrier. The increase of diffusion barrier can be attributed to many factors, such as the increased electrostatic repulsion between Li/Na atoms, the volume expansion and lattice distortion in high Li/Na concentration. Furthermore, the energy barriers of Li are smaller than that of Na in both bulk and monolayer TiS_3 due to its smaller radius. Our results suggest that the Li/Na diffuses slowly as the increase of Li/Na concentration.
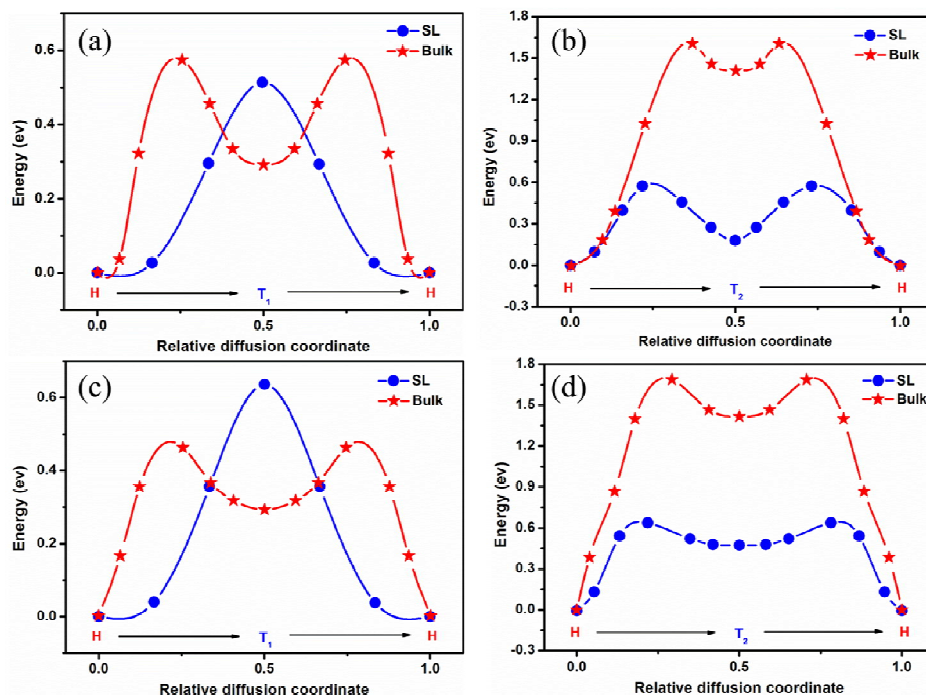
Fig. 8 Energy barrier (∇E) for Li ((a) and (b)) and Na ((c) and (d)) atoms diffuse along H-T$_1$-H and H-T$_2$-H pathways in bulk and monolayer TiS$_3$ with Li/Na atoms absorbed the whole H sites except an unoccupied H site, respectively.

In order to know the capacity of Li/Na in bulk and monolayer TiS$_3$, we calculated the maximum Li/Na concentration. Based on our calculations, we found that bulk TiS$_3$ can accommodate 2 Li/Na, occupying all the H, T$_1$ and T$_2$ sites. As a result, 339 and 282 mAh/g for Li and Na storage were obtained in bulk TiS$_3$. However, in the case of monolayer TiS$_3$, although the theoretical capacity of 488 and 377 mAh/g for Li and Na storage if all three adsorption sites are occupied, only 1.5 Li/Na can be adsorbed due to the serious structure deformation and weaker bonding strength of Li/Na at higher Li/Na concentrations. Consequently, the capacities of monolayer TiS$_3$ are 260 and 225 mAh/g for Li and Na, respectively.

We further calculate the volume changes for the insertion of 1, 1.5 and 2 Li/Na atoms in bulk TiS$_3$, respectively. (**Fig. S1**) It shows that the volume of bulk TiS$_3$ expands with increasing Li/Na concentrations, and Na shows higher volume expansion than Li. In the case of 2 Li/Na atoms in bulk TiS$_3$, volumes expanses by about 33 and 57% for Li/Na, respectively. Meanwhile, the bond length of two single-bonded disulfide ions (S$_2^{2-}$) is broken from 2.04 Å to 3.06 Å and 3.19 Å for Li/Na, respectively, in agreement with the experimental result.[13] (**Fig. S2**)
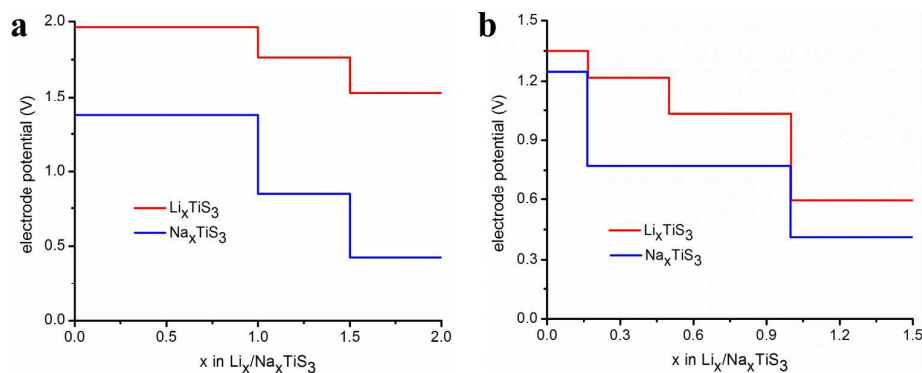
Fig. 9 Electrode potential of Li/Na-intercalated (a) bulk and (b) monolayer TiS$_3$ against Li/Li$^+$ and Na/Na+, respectively.

To explore more information on the TiS$_3$ as electrode material for Li and Na batteries, we calculated the voltage profile, the electrode potential V respect to Li/Li+ and Na/Na+ are expressed as follows,[44, 45]

$$V(Li/Na) = -\frac{E(Li_{x2}TiS_3) - E(Li_{x1}/Na_{x2}TiS_3) - (x_2 - x_1)E(Li/Na)}{x_2 - x_1}$$

where E is the total energy, E(Li/Na) is the energy per atom of Li/Na in the bcc crystal, and x is the number of Li/Na atoms. **Fig. 9** shows the concentration-dependent of the electrode potential of Li/Na-intercalated in bulk and monolayer TiS$_3$ against Li/Li$^+$ and Na/Na+, respectively. In bulk TiS$_3$, the voltage profile for LiTiS$_3$ is in a range of 1.5-2.0 V, and two plateau appear between LiTiS$_3$- Li$_{1.5}$TiS$_3$，Li$_{1.5}$TiS$_3$- Li$_2$TiS$_3$, agree well with experimental results.[13] The plateaus for Li and Na in monolayer TiS$_3$ are lower than that in bulk TiS$_3$. Moreover, in both bulk and monolayer TiS$_3$, the plateaus against Li/Li$^+$ are higher than that of against Na/Na+, which also exits in MoS$_2$ systems.[46]

From the above discussions, monolayer TiS$_3$ shows a potential application in practical lithium batteries. However, because of the lower voltage of monolayer Li$_x$TiS$_3$ compared to bulk, the weaker constraint of the surface S are more likely to react with Li or Na adatoms. Thus, it is essential for us to confirm the thermodynamic stability of monolayer Li$_x$TiS$_3$ or Na$_x$TiS$_3$ within the charge-discharge process. The safety problem in metal sulfides often arises from the interaction of the highly charged S^{2-} with the gradually filled Li/Na atoms. Recently, Lemmon and co-workers[47] reported that MoS$_2$ was reduced to metallic Mo and Li$_2$S at 0.01 V (vs. Li$^+$/Li). Fang et al.[48] suggested that the lithium storage mechanism of MoS$_2$ could be expressed as MoS$_2$ + xLi$^+$ + xe $\rightarrow$ Li$_x$MoS$_2$ (above 1.00 V), and then followed by Li$_x$MoS$_2$ + (4-x)Li$^+$ +(4-x)e$^-$ $\rightarrow$ Mo + Li$_2$S (0.01 V). Moreover, similar reaction mechanism was also found in the SnS$_2$ system.[49] In TiS$_3$ system, when a large amount of S$_2^{2-}$ is present, these particularly unstable reduction states have the potential to further reduce by liberating S to form the energetic stable Li$_2$S, yielding the great loss of active mass of the electrode and consequently a much limited cycle life of the battery. The intrinsic thermal stability of TiS$_3$ can be understood by the following decomposition reaction

$$A_xTi_{12}S_{36} + 2A = A_xTi_{12}S_{35} + A_2S$$
$$\Delta E = E^0(A_xTi_{12}S_{35}) + E^*(A_2S) - E^0(A_xTi_{12}S_{36}) - 2E(A)$$

where A indicates the alkali metal atoms (Li, Na), E^0 refers to the total energy at 0 K, $E(A)$ is the total energy of Li/Na atom in bcc structure, and $E^*(A_2S)$ is the calculated energy of an Li_2S molecule. The formation energy of the reaction for each stage is shown in **Fig. S3**. Formation energy of Li_2S and Na_2S monotonically increases as a function of x, which indicates the upward trend in stability of both $Li_xTi_{12}S_{36}$ and $Na_xTi_{12}S_{36}$ ($0 \leq x \leq 1.5$) with the increase of x. The positive ΔE means that the formation of Li_2S and Na_2S is thermodynamically infeasible. It can be seen that ΔE is always positive, thus the reaction is not thermodynamically possible. Such results suggest that monolayer TiS_3 has high stability, at least from the energetic point of view.

4. Conclusions

In this paper, first-principle calculations have been used to study the electronic properties of bulk and monolayer TiS_3 and its characteristics as electrode materials in rechargeable Li and Na ion batteries. The investigation of the electronic structure reveals that both bulk and monolayer TiS_3 are semiconductors with a band gap of about 1 eV, but as the thickness of the TiS_3 material decreases to a monolayer, a transition from an indirect band gap to a direct band gap occurs. The investigation on the adsorption and diffusion properties of Li and Na atoms in bulk TiS_3 reveals that the energy diffusion barriers for both are low, and after absorption of Li and Na in bulk TiS_3, Na shows higher expansion lattice parameters than Li. However, the volume expansion problem can be neglected in monolayer structures. Furthermore, the Li/Na mobility on monolayer TiS_3 is improved along the H-T_2-H pathway. The bulk TiS_3 can accommodate 2 Li/Na, slightly higher than that of monolayer TiS_3 of 1.5 Li/Na, corresponding to 339 and 282 mAh/g for Li and Na storage, respectively. Our calculated plateaus for Li in bulk TiS_3 are in agreement with experiment. The plateaus for Li and Na in bulk TiS_3 are higher than that in monolayer TiS_3. Moreover, the plateaus against Li/Li^+ are higher than that of against Na/Na+. In conclusion, our work confirms the following: (1). Bulk and monolayer TiS_3 are semiconductors with low diffusion barriers and are therefore suitable materials for ion batteries. (2). Na is a viable replacement material for Li in TiS_3, where Na shows better diffusion performance than Li. (3). The monolayer TiS_3 shows improved Na ion batteries performance with smaller structure expansion compared with their bulk counterpart. (4). In bulk TiS_3 with high Li/Na concentration, there is only one diffusion pathway, which is useful for directed diffusion.

Acknowledgments

Notes and References

1. H. S. Kim, T. S. Arthur, G. D. Allred, J. Zajicek, J. G. Newman, A. E. Rodnyansky, A. G. Oliver, W. C. Boggess and J. Muldoon, *Nat. Commun.*, 2011, **2**, 427.
2. M. S. Whittingham, *Science*, 1976, **192**, 1126.
3. L. Yu, L. Zhang, H. B. Wu and X. W. Lou, *Angew. Chem. Int. Ed.*, 2014, **53**, 3711.
4. A. Sakuda, N. Taguchi, T. Takeuchi, H. Kobayashi, H. Sakaebe, K. Tatsumi and Z. Ogumi, *Electrochem. Commun.*, 2013, **31**, 71.
5. J. J. Ma, X. Y Liu, X. J Cao, S. H. Feng and M. E. Fleet, *Eur. J. Inorg. Chem.*, 2006, **2006**, 519.
6. V. Nicolosi, M. Chhowalla, M. G. Kanatzidis, M. S. Strano and J. N. Coleman, *Science*, 2013, **340**, 6139.
7. Z. Y. Zeng, C. L. Tan, X. Huang, S. Y. Bao and H. Zhang, *Energy Environ. Sci.*, 2014, **7**, 797.
8. C. T. Li, C. P. Lee, Y. Y. Li, M. H. Yeh and K. C. Ho, *J. Mater. Chem. A*, 2013, **1**, 14888.
9. N. A. Kyeremateng, N. Plylahan, A. C. S. dos Santos, L. V. Taveira, L. F. P. Dick and T. Djenizian, *Chem. Commun.*, 2013, **49**, 4205.
10. M. S. Whittingham, *Prog. Solid State Chem.*, 1978, **12**, 41.
11. J. E. Trevey, C. R. Stoldt and S. H. Lee, *J. Electrochem. Soc.*, 2011, **158**, A1282.
12. C. M. Julien, *Mater. Sci. Eng., R,* 2003, **40**, 47.
13. M. H. Lindic, H. Martinez, A. Benayad, B. Pecquenard, P. Vinatier, A. Levasseur and D. Gonbeau, *Solid State Ionics*, 2005, **176**, 1529.
14. A. Hayashi, T. Matsuyama, A. Sakuda and M. Tatsumisago, *Chem. Lett.*, 2012, **41**, 886.
15. Y. J. Kim, Y. Kim, A. Choi, S. Woo, D. Mok, N. S. Choi, Y. S. Jung, J. H. Ryu, S. M. Oh and K. T. Lee, *Adv. Mater.*, 2014, **26**, 4139.
16. S. Y. Hong, Y. Kim, Y. Park, A. Choi, N. S. Choi and K. T. Lee, *Energy Environ. Sci.*, 2013, **6**, 2067.
17. V. Palomares, P. Serras, I. Villaluenga, K. B. Hueso, J. Carretero-González and T. Rojo, *Energy Environ. Sci.*, 2012, **5**, 5884.
18. V. V. Kulish, O. I. Malyi, M. F. Ng, Z. Chen, S. Manzhos and P. Wu, *Phys. Chem. Chem. Phys.,* 2014, **16**, 4260.
19. Z. Margherita, J. L. Shaw and G. J. Tennenhouse, *J. Electrochem. Soc.*, 1981, **128**, 1647.

20. M. S. Xu, T. Liang, M. M. Shi and H. Z. Chen, *Chem. Rev.*, 2013, **113**, 3766.

21. J. O. Island, M. Buscema, M. Barawi, J. M. Clamagirand, J. R. Ares, C. Sánchez, I. J. Ferrer, G. A. Steele, H. S. J. van der Zant and A. Castellanos-Gomez, *Adv. Optical Mater.*, 2014, **2**, 641.

22. I. J. Ferrer, J. R. Ares, J. M. Clamagirand, M. Barawi and C. Sánchez, *Thin Solid Films*, 2013, **535**, 398.

23. J. Carrasco, *J. Phys. Chem. C*, 2014, **118**, 19599.

24. Y. Z. Chen, F. Peng, Y. Yan, Z. W. Wang, C. L. Sun and Y. M. Ma, *J. Phys. Chem. C*, 2013, **117**, 13879.

25. G. C. Yang, Y. C. Wang and Y. M. Ma, *J. Phys. Chem. Lett.*, 2014, **5**, 2516.

26. J. Zhou, Q. Wang, Q. Sun and P. Jena, *J. Phys. Chem. C*, 2011, **115**, 6136.

27. M. Kan, J. Y. Wang, X. W. Li, S. H. Zhang, Y. W. Li, Y. Kawazoe, Q. Sun and P. Jena, *J. Phys. Chem. C*, 2014, **118**, 1515.

28. D. Wang, L.-M. Liu, S.-J. Zhao, B.-H. Li, H. Liu and X.-F. Lang, *Phys. Chem. Chem. Phys.*, 2013, **15**, 9075.

29. G. Kresse and J. Furthmüller, *Phys. Rev. B*, 1996, **54**, 11169.

30. G. Kresse and J. Furthmüller, *Comput. Mater. Sci.*, 1996, **6**, 15.

31. J. P. Perdew, K. Burke and M. Ernzerhof, *Phys. Rev. Lett.*, 1996, **77**, 3865.

32. H. J. Monkhorst and J. D. Pack, *Phys. Rev. B*, 1976, **13**, 5188.

33. A. V. Krukau, O. A. Vydrov, A. F. Izmaylov and G. E. Scuseria, *J. Chem. Phys.*, 2006, **125**, 224106.

34. X. Wu, M. C. Vargas, S. Nayak, V. Lotrich and G. Scoles, *J. Chem. Phys.*, 2001, **115**, 8748.

35. A. Togo, F. Oba and I. Tanaka, *Phys. Rev. B*, 2008, **78**, 134106.

36. M. E. Fleet, S. L. Harmer, X. Liu and H. W. Nesbitt, *Surf. Sci.*, 2005, **584**, 133.

37. H. G. Grimeiss, A. Rabenau, H. Hahn and P. Ness, *Z. fur Elecktrochem*, 1961, **65**, 776.

38. Q. Li, D. Zhou, W. T. Zheng, Y. M. Ma and C. F. Chen, *Phys. Rev. Lett.*, 2013, **110**, 136403.

39. W. J. Yin, Y. E. Xie, L. M. Liu, R. Z. Wang, X. L. Wei, L. Lau, J. X. Zhong and Y. P. Chen, *J. Mater. Chem. A*, 2013, **1**, 5341.

40. H. Zhang, L. M. Liu and W. M. Lau, *J. Mater. Chem. A*, 2013, **1**, 10821.

41. S. Z. Butler, S. M. Hollen, L. Y. Cao, Y. Cui, J. A. Gupta, H. R. Gutiérrez, T. F. Heinz, S. S. Hong, J. Huang, A. F. Ismach, E. Johnston-Halperin, M. Kuno, V. V. Plashnitsa, R. D. Robinson, R. S. Ruoff, S. Salahuddin, J. Shan, L. Shi, M. G. Spencer, M. Terrones, W. Windl and J. E. Goldberger, *ACS Nano*, 2013, **7**, 2898.

42. R. F. W. Bader, in *Encyclopedia of Computational Chemistry*, John Wiley & Sons, Ltd, 2002.

43. G. Henkelman, A. Arnaldsson and H. Jónsson, *Comput. Mater. Sci.*, 2006, **36**, 354.

44. M. K. Aydinol, A. F. Kohan, G. Ceder, K. Cho and J. Joannopoulos, *Phys. Rev. B*, 1997, **56**, 1354.

45. M. K. Aydinol, A. F. Kohan and G. Ceder, *J. Power Sources*, 1997, **68**, 664.

46. M. Mortazavi, C. Wang, J. K. Deng, V. B. Shenoy and N. V. Medhekar, *J. Power Sources*, 2014, **268**, 279.

47. J. Xiao, D. Choi, L. Cosimbescu, P. Koech, J. Liu and J. P. Lemmon, *Chem. Mater.*, 2010, **22**, 4522.

48. X. P. Fang, X. W. Guo, Y. Mao, C. X. Hua, L. Y. Shen, Y. S. Hu, Z. X. Wang, F. Wu and L. Q. Chen, *Chem– Asian J*, 2012, **7**, 1013.

49. I. Lefebvre-Devos, J. Olivier-Fourcade, J. C. Jumas and P. Lavela, *Phys. Rev. B*, 2000, **61**, 3110.